# A New Nonlinear Compliant Mechanism for Harvesting Energy from Ocean Waves

Haitong Liang
School of Engineering and Architecture-Electrical and Electronic Engineering,
Tyndall National Institute
University College Cork
Cork, Ireland
haitong.liang@tyndall.ie

Matias Carandell Widmer
SARTI Group,
Electronic Engineering Department
Universitat Politècnica de Catalunya
Vilanova i la Geltrú, Spain
matias.carandell@upc.edu

Oskar Z. Olszewski
Piezo-MEMS Group,
Tyndall National Institute
Cork, Ireland
zbigniew.olszewski@tyndall.ie

Guangbo Hao
School of Engineering and Architecture-Electrical and Electronic Engineering,
Tyndall National Institute
University College Cork
Cork, Ireland
G.hao@ucc.ie

**Abstract**—Traditonal linear oscillators, such as cantilevers or pendulums, are only sensitive to specific resonant frequencies. They have then very narrow frequency bandwidths when harvesting energy from ocean waves. In order to enhance the dynamic performance of the wave energy converters (WECs), used to expand the autonomy of Lagrangian Drifters, a statically balanced compliant mechanism (SBCM) is investingated. It is based on finite element analysis (FEA) simulaitons. The design of the SBCM is introduced and its static force-displacement curve is obtained in FEA. The dynamic response of the SBCM to harmonic base excitiaons at low frequencies and low accelerations is investigated based on time-domian FEA simulations. The close agreement between simulations, numerial and analytical results verifies that the SBCM is sensitive to ultra-low frequencies with weak accelerations in a wide frequency range. The applicability of the SBCM in WECs is demonstrated by adding PVDF films in the FEA model. In the time-domian simulation, the SBCM-based WEC is excited by the drifter motion pattern obtained from Orcaflex and corresponding to two typical ocean waves (i.e. synthesized Airy and Jonswap models). Relative displacement between the base and mass and the electric outputs are obtained. According to this work, the SBCM provides a structural solution for WECs with enhanced energy harvesting performance.

***Keywords***— *Lagrangian Drifter, Wave Energy Converter (WEC), Compliant mechanism, Stiffness nonlinearity, Wide bandwidth, FEA simulation.*

## I. Introduction

MARINE biodiversity is highly affected by global warming. Almost 90% of the heat produced during the last decade has been absorbed by oceans, destroying many marine ecosystems. Closely tracking ocean changes helps prevent the effects of this phenomenon and maintain the Earth's health. Oceanographic sensor platforms provide biological and meteorological data to help understand changes in marine environments. Underwater cabled observatories [1] or autonomous underwater vehicles [2] are sensor platforms that provide a large quantity of data but entail high deployment and maintenance costs.

Lagrangian drifters (Fig. 1) are autonomous floating passive devices used in marine climate research that provide surface marine data [3]. They are low-cost, versatile and easy-to-deploy instrumentation, so many of them can be deployed in large oceanic regions forming a surface sensors network. Drifter deployments can last for years, so autonomy is one of the leading design challenges [4]. Several Energy Harvesting (EH) sources are being explored to reduce costs in battery replacement maintenance tasks. Solar panels have been the most common commercial solution for expanding a drifter's autonomy (Sofar: Spotter, Fastwave: Voyager Solar). Drifters must avoid the impact of the wind because this may compromise a proper superficial current tracking [5]. Consequently, they must be mostly submerged, interfering with the feasibility of solar harvesting. Depending on a single EH source will have little effect on making the unit more autonomous. For this reason, other EH sources are being explored, including the oscillatory movement of the drifter itself caused by the interaction with the ocean waves.

References [6]–[9] present different Wave Energy Harvesters (WECs) based on electromagnetic techniques to convert vibrational energy into electricity. Specifically in

Fig. 1. Lagrangian Drifter deployed at coastal area, in the Mediterranean Sea, within the tests of the EC-founded MELOA project [3].

This work was funded by the European Union's Horizon 2020 projects EnABLES, grant agreement No.730957 and MELOA, grant agreement No. 776280. The first author has a grant from EnABLES project (No.730957). The second author has a grant from the Secretariat of Universities and Research of the Ministry of Business and Knowledge of the Government of Catalonia on the FI program (ref. BDNS 362582).

[10], a novel pendulum-type WEC which uses the motion of waves and the current flow to generate power from a drifter was presented. The WEC consists of an articulated pendulum arm with a proof mass that transforms the oscillation into rotation and electic outputs are obtaind from a DC generator. In [11], it has been experimentally proven that embedding a moving element in a drifter does not affect its ocean measurements as long as the EH mass is small enough in relation to that of the drifter. Piezoelectric capacitors are also popular choices for energy conversion in WECs [12]. However, the linear oscillators used in all these WEC's systems lead to an unefficient narrow frequency bandwidth. Since ocean waves have mixed frequencies in a low frequency range with weak accelerations, the resulting performance of the system would be far from its optimum point and would present low conversion efficiency.

Mehcanial structures act as interfaces between the drifter virbaitons and the energy-conversion capacitors in the WECs [13]. In order to enhance the dynamic performance and the energy generation capability, a Statically Balanced Compliant Mechanism (SBCM) is proposed as a structural solution for WECs embedded in drifters. This SBCM is able to stay in equilibrium in the continuous static-balancing displacement range, while it owns nonlinear stiffness in the wider displacement range. Due to its unique nonlinear force-displacement characteristics, the SBCM responds to ultra-low frequencies with weak accelerations in a wide frequency range. Other advantages of the SBCMs include highly-alleviated friction, less or no assembling procedure, reduced mass, low cost and good manufacturability. They all benefit the application into WECs [14], [15]. This paper investigates the dynamic performance of the proposed SBCM under harmonic exciations based on FEA simulations with COMSOL. The applicability of the SBCM in WECs is also demonstrated utilizing the drifter motion patterns generated from Orcaflex as displacement excitations in FEA simulations.

The paper is organized as follows: Section II describes the design of the SBCM and the analytical results of the dynamic response to harmonic base excitaitons. Section III presents the FEA simulation on the SBCM model unerder harmonic base excitations at discrete frequency points in the low frequency range. Section IV presents the simulation of a drifter in the sea using a commercial software (OrcaFlex). The applicability of the SBCM in WECs is demonstrated by adding a PVDF in the FEA model and exciting it with the difter motion patterns. Conslusions are drawn in the last section.

## II. THE STATICALLY BALANCED COMPLIANT MECHANISM

### A. Design of the SBCM

SBCMs are mainly designed based on the stiffness compensation between the positive-stiffness components and the negative-stiffness components [16], [17]. In the SBCM presented in this work, the positive-stiffness component is embodied using a pair of double parallelogram mechanisms connected in parallel. The negative-stiffness component is composed of two pairs of the fixed-guided post-buckled compliant beams in by-symmetry. Fig. 2 shows the 2D FEA model of the SBCM created in COMSOL. In the FEA simulation, the axial preloading on the negative-stiffness beams is achieved with the Contact and Adhesion functions of COMSOL. In addition, the negative-stiffness beams are designed with a curvature with the radius of 5000 mm to ensure the beams buckle to the opposite directions and avoid interference during oscillation.

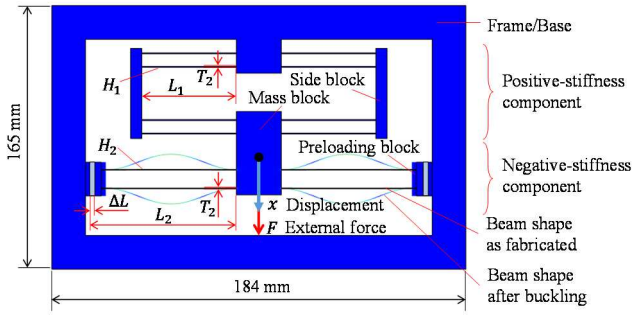


Fig. 2. Schematic structure of the SBCM.

The structural steel is selected as the material in the FEA model. $L_1$, $T_1$ and $H_1$ are respectively length, (in-plane) thickness and width (out-of-plane thickness) of the positive-stiffness beams. $L_2$, $T_2$ and $H_3$ are the corresponding geometric parameters of the negative-stiffness beams. $\Delta L$ is the displacement preloading applied on the negative-stiffness beams. Positive and negative-stiffness components are connected through the sharing mass block in the center position. $F$ is the external force applied on the movable mass block and $x$ is the relative displacement between the mass block and the frame caused by the external force. The force-displacement of the compliant structure is simulated and plotted with prescribed displacement function in COMSOL. Static balancing is finally achieved by finely tuning the geometric parameters and the resulting force-displacement curve between -11 mm and 11 mm is plotted as a solid line in Fig. 3. The corresponding geometric parameters of the SBCM in its static-balancing status is listed in TABLE I. In the displacement range between -1.8 mm and 1.8 mm, the corresponding force is very close to zero (smaller than 0.01 N) which can be considered as static balancing in this work. Note that the parameters given in TABLE I is just one example of many possible geometric solutions in different scales.

TABLE I. Geometric parameters of the SBCM with static balancing achieved based on FEA simulation.

| Positive-stiffness component | | Negative-stiffness component | |
|---|---|---|---|
| $L_2$ | 42 mm | $L_2$ | 60 mm |
| $H_2$ | 15 mm | $H_2$ | 15 mm |
| $T_2$ | 0.4 mm | $T_2$ | 0.3 mm |
| —— | —— | $\Delta L$ | 2 mm |

In order to describe the force-displacement link on the SBCM, the force-displacement curve is fitted with a polynomial equation with Polyfit function in Matlab. Fig. 3 shows that the force-displacement curve is symmetric about the origin point. Therefore, only odd order terms exist in theory and odd order terms are neglected in the polynomial equation as shown in Eq. (1).The fitting curve is also shown in Fig. 3 indicated with a dashed line. The $R^2$ coefficient of

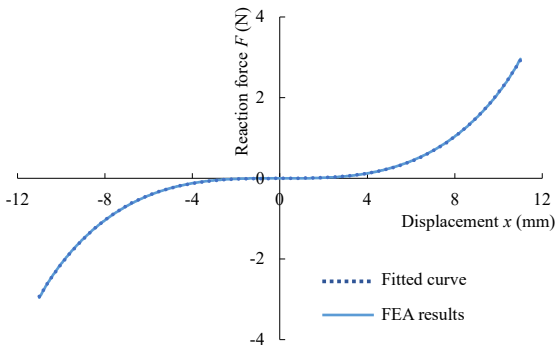


Fig. 3. Force-displacement curve of the SBCM.

determination is 99.94 %, which indicates an accurate fit of this polynomial equation to the force-displacement curve obtained from the FEA simulation.

$$F(x) = 0.002194x + 0.001774x^3 + 0.000003362x^5 \quad (1)$$

### B. *Theoretical dynamic modeling of the SBCM*

The static force-displacement characteristic of the SBCM determines its dynamic response to external excitations. The relative displacement between the mass block and the frame is directly related to the performance of the SBCM in EH applications. Therefore, it is concerned and focused in this work. In order to describe the force-displacement link of the SBCM, a polynomial 5 degree equation with only odd order terms is proposed as Eq. (2).

$$F(x) = \alpha x + \beta x^3 + \gamma x^5 \quad (2)$$

where $\alpha$, $\beta$ and $\gamma$ are the coefficients of the odd-order terms. Based on this general force-displacement equation, the dynamic motion equation of the SBCM under harmonic base excitation can be described as:

$$-m\ddot{z} = m\ddot{x} + c\dot{x} + \alpha x + \beta x^3 + \gamma x^5 \quad (3)$$

where $m$ is mass of the movable block, $c$ is the damping ratio of the system, $x$ represents the steady-state relative displacement between the mass block and the frame, $\ddot{z}$ is the base excitation acceleration assumed to be $\ddot{z} = A_0 cos(\Omega t)$.

To facilitate analysis, Eq. (3) can be formulated as:

$$-A_0 cos(\Omega t) = \ddot{x} + 2\zeta\dot{x} + k_1 x + k_2 x^3 + k_3 x^5 \quad (4)$$

where the individual coefficients can be expressed by the following formulae:

$$2\zeta = \frac{c}{m}, \quad k_1 = \frac{\alpha}{m}, \quad k_2 = \frac{\beta}{m}, \quad k_3 = \frac{\gamma}{m}$$

Based on the averaging method, the relationship between the relative base-mass displacement ($H$) and the excitation frequency ($\Omega$) can be obtained. This H-$\Omega$ relationship can also be obtained numerically based on Eq. (4) with the ODE-45 MATLAB function. In the FEA model created, the mass of the mass block is 88.8 g and the damping ratio ($\zeta$) is 1.7. Under the harmonic base excitation in the ultra-low frequency range from 0.25 Hz to 20 Hz with a weak acceleration of 0.25 g and 0.5 g, the analytical and numerical results of the *H-Ω* relationship of the SBCM in its static-balancing status are plotted in Fig. 4. These theoretical results show that this SBCM responds to ultra-low excitation frequencies (theoretically starting from 0 Hz) in a wide frequency range. The maximum relative displacement amplitude can reach 20 mm at 13 Hz and 0.5 g.

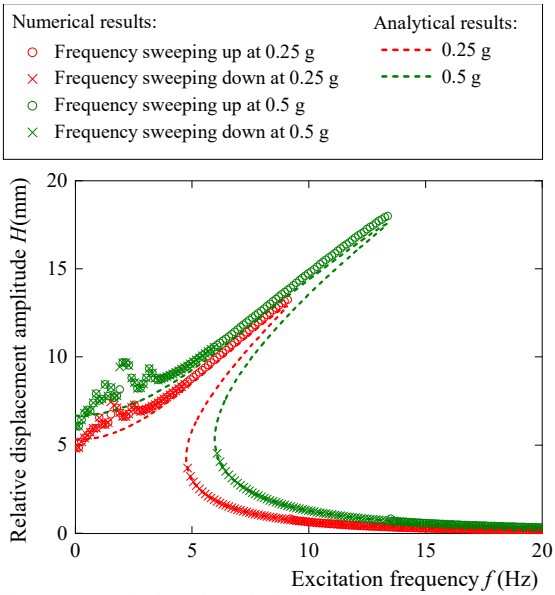


Fig. 4. Numerical and analytical results of the dynamic relative displacement response of the SBCM in the ultra-low excitation frequency range from 0.25 Hz to 10 Hz with the accelerations of 0.25 g and 0.5 g.

## III. FEA SIMULATION ON THE SBCM WITH HARMONIC EXCITATIONS.

### A. *Harmonic base excitation with acceleration of 0.25 g.*

The dynamic response of the proposed SBCM under sinusoidal excitations with ultra-low frequencies and weak accelerations is explored based on FEA simulations. The excitation frequency range is set from 0.25 Hz to 10 Hz according to the frequency spectrum of ocean waves studied in [18], with two acceleration values of 0.25 g and 0.5 g (1 g equals to 9.8 m/s$^2$). Base excitation is applied on the outer frame of the model by the "Prescribed Displacement" boundary condition in the time domain for 20 periods. Regarding to a given frequency and an acceleration (e.g. 1 Hz, 0.25 g), one simulation is carried out. The simulated relative displacement between the mass and base ($H$), the absolute displacement of the base ($x_{base}$) and the absolute displacement of the mass ($x_{mass}$) are captured and plotted with respect to time ($t$).

The displacement curves of the SBCM under the excitation condition of 3 Hz and 0.25 g in time domain are presented in Fig. 5 as an example of the dynamic FEA simulation results. The response displacement of the mass block is illustrated as a blue curve and the average amplitude is about 14 mm. The red curve is the relative displacement between the base and frame and its average amplitude is about 7.57 mm. $H$ is focused in the FEA simulation since it directly influences the performance of the SBCM. Regarding to the excitation frequencies in the range from 0.25 Hz to 10 Hz with the acceleration of 0.25 g and 0.5 g, $H$ is collected and summarized in TABLE II. It should be noted that the average relative displacement amplitude of 10 continuous oscillations in its steady state at each frequency point is recorded as the relative displacement amplitude ($H$). Based on the data in TABLE II, the *H-Ω* curve is shown in Fig. 6.

TABLE II. Relative displacement of the SBCM under harmonic base excitaitons in the dynamic FEA simulations.

| Base excitation frequency $f$ (Hz) | Relative displacement amplitude $H$ (mm) at 0.25 g | Base excitation frequency $f$ (Hz) | Relative displacement amplitude $H$ (mm) at 0.5 g |
|---|---|---|---|
| 0.25 | 5.4 | 0.25 | 7.32 |
| 0.5 | 5.19 | 0.5 | 6.73 |
| 1 | 5.86 | 1 | 6.5 |
| 2 | 6.67 | 2 | 9.4 |
| 3 | 7.57 | 3 | 9.83 |
| 4 | 8.04 | 4 | 10.28 |
| 5 | 1.26 | 5 | 10.93 |
| 6 | 1.21 | 7 | 1.77 |
| 8 | 0.53 | 9 | 1.19 |
| 10 | 0.35 | 10 | 0.44 |

Fig. 6 shows and compares the *H-Ω* curves of the SBCM under the harmonic base excitation with acceleration of 0.25 g and 0.5 g obtained from FEA simulations, analytical and numerical results. A close agreement between these three methods is observed in the frequency range from 0,25 Hz to 10 Hz, which is also the frequency domain of ocean waves. It

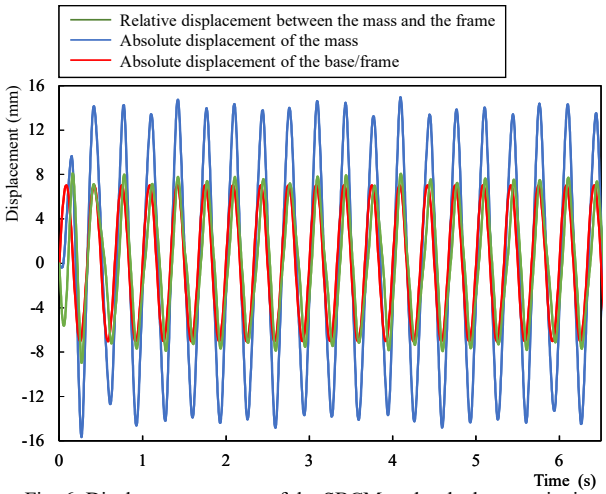


Fig. 6. Displacement curves of the SBCM under the base excitation at 3 Hz, 0.25 g in FEA simulation

is concluded that the SBCM is sensitive to ultra-low wide bandwidth excitation frequencies with weak accelerations. The SBCM investigated in this paper provides a suitable structural solution in harvesting vibrational energy from ocean waves.

Notice that large displacement amplitudes have not been obtained in FEA simulations at excitation frequencies between the jumping-up and jumping-down frequencies. FEA simulation is carried out at discrete frequencies with no vibrational "history". I.e. vibrational energy from previous oscillation status is considered as initial conditions. In real operation with SBCM prototypes, external disturbing can be applied to the oscillating mass block to stimulate the oscillation with larger amplitude, while this is not available in FEA simulations.

When the excitation frequency is higher than the jumping-up frequencies (Fig. 6), H jumps significantly and large amplitudes observed in analytical and numerical results cannot be researched in FEA simulations. This is because FEA simulation is carried out at discrete frequencies with no vibrational "history". In real operation, external disturbing can be applied to the oscillating mass block and the vibration status with larger amplitude can be stimulated from the

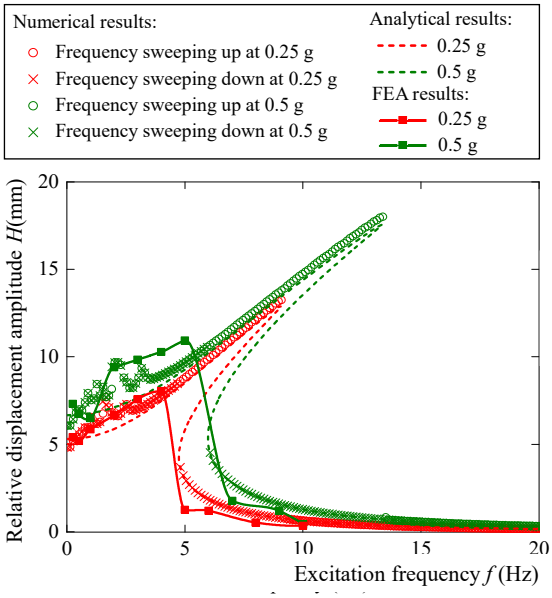


Fig. 7. H-Ω curves of the SBCM based on the FEA simulation, analytical modelling and numerical analysis under the base excitation acceleration of 0.25 g and 0.5 g.

vibration status with smaller vibration amplitude. The essence of the external disturbing here is imported energy to the oscillation system. However, this operation is not available or very complex in the FEA simulation.

## IV. Voltage Output Demonstration Based on Drifter Motion Patterns.

The applicability of the proposed SBCM in energy harvesting from ocean waves is explored in this section based on FEA simulations. The FEA model of a preliminary SBCM-based PVEH is created with piezoelectric materials applied on the flexural beams. PVDF films are used as piezoelectric components for energy conversion due to their good piezoelectric performance and outstanding flexibility. Two pieces of PVDF films (20 mm×15 mm ×0.2 mm for each) are added symmetrically in the near-root area of the upper positive-stiffness beams, on the side close to the central fixing position (Fig. 7). Drifter motion patterns corresponding to typical ocean waves are used as displacement base excitations in the time domain FEA simulaiton. The voltage output across an external resistance of 1 MΩ and relative displacement of the SBCM are are measured and plotted.

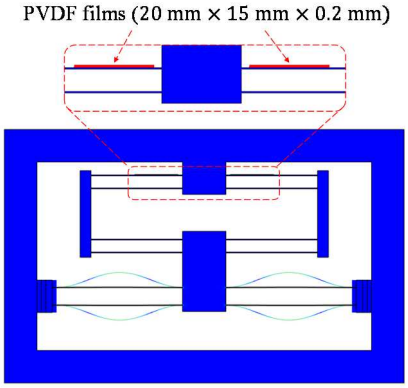


Fig. 5. FVDF films and their attachment positions in the FEA model.

### A. Drifter dynamics under wave excitation

The drifter motion has been simulated in OrcaFlex. It is a dynamic analysis software for offshore marine systems used to understand the interaction between the sea waves and the drifter and help design a successful WEC. This package has been used to emulate an ocean with common swell conditions and provide the vectors of motion of a free-floating buoy. These motion patterns have then been used as the base displacement excitations in the FEA simulations.

The spherical drifter has been modeled with the parameters shown in TABLE III, using 24 stacked, flat cylinders of appropriate diameters. Fig. 8 shows the resulting modeled drifter with the location of its local axis origin at the center of the sphere, where the WEC should be attached. The drifter has a spherical shape of 10 cm radius ($R$) and weighs 3.6 kg ($m_b$). This results in an overhang of 5 cm from the Still Water Line (SWL) in rest conditions ($d$), reducing the impact

TABLE III. Ocean drifter parameters

| Symbol | Parameter | Value | Units |
|---|---|---|---|
| $m_b$ | Mass | 3.6 | kg |
| $R$ | Radius | 0.1 | m |
| $c_m$ | Centre of mass[A] | -0.05 | m |
| $d$ | SWL- $c_g$ distance | 0.05 | m |
| $I_Y$ | Horizontal inertia | $9 \cdot 10^{-3}$ | Kg·m$^2$ |

[A]Center of mass below the drifter's geometric center.

of the wind in the drifter's shell. Placing the battery pack below the drifter's geometric center shifts its center of mass ($c_m$) downwards by 5 cm, making the drifter stable and thus ensuring the antenna is always above the waterline.

The sea state has been modeled using two sea models to estimate the performance of the WEC in both conditions. On the one hand, a regular sea implemented with the Airy model [19], a sinusoidal-shape trajectory that simply describes the surface particle motion. This is defined by the significant wave height ($H_S$) and the significant wave period ($T_Z$). This sea model has been composed of the superposition of two regular waves. On the other hand, an irregular sea state is described by the JONSWAP model [20]. JONSWAP spectrum is a water wave model that statistically describes the behavior of the water particles in shallow waters, resulting in a bandwidth distribution of frequencies around the main one ($1/T_Z$). TABLE IV summarizes both models and the shared environmental parameters.

TABLE IV. Environment parameters

| Sea model | Symbol | Parameter | Value | Units |
|---|---|---|---|---|
| - | $h$ | Ocean depth | 20 | m |
| - | $\rho$ | Ocean density | 1024 | Kg/m$^3$ |
| - | $g$ | Gravity accel. | 9.81 | m/s$^2$ |
| *Regular*[B] | $H_{S1}$ | Sig. Wave Height | 0.7 | m |
| | $T_{Z1}$ | Sig. Wave Period | 3.5 | s |
| | $H_{S2}$ | Sig. Wave Height | 1.5 | m |
| | $T_{Z2}$ | Sig. Wave Period | 8 | s |
| *Irregular* | $H_{S3}$ | Sig. Wave Height | 0.8 | m |
| | $T_{Z3}$ | Sig. Wave Period | 3 | s |

[B]REGULAR SEA MODEL COMPOSED BY THE SUPERPOSITION OF TWO REGULAR WAVES.

Fig. 8 defines also the global axis, where Y is the horizontal axis and Z is the vertical axis. It also defines the concepts of wave height ($H$) and period ($T$) among the SWL. For simplicity, the wave propagation direction has been aligned with the horizontal drifter's local axis Y, leading to a simpler model of 2D. The interaction with the wave motion causes the drifter's vertical displacement ($D_Z$) which is the vector that has been later used as excitation in FEA simulations.

Simulation results are shown in Fig. 9, where the vertical drifter displacement is shown for both sea models. Orange has been used for the Airy model and blue for the JONSWAP model. The left side of the figure contains the time-domain results and the right side contains the frequency-domain results (FFT function has been used for this purpose). Airy $D_Z$ presents a composition of two sinusoidal waves at a different

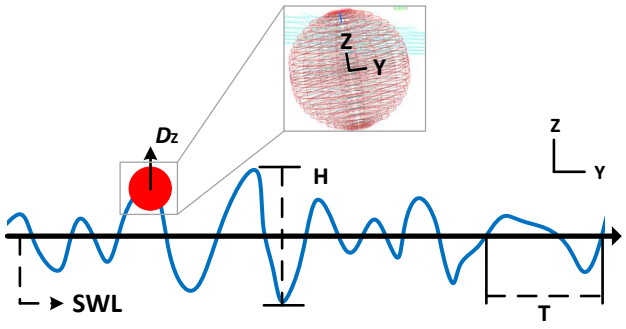


Fig. 8. 2D scheme of the drifter's motion with the description the main wave's parameters. Zoom in of the spherical modelling of the drifter in OrcaFlex, using 24 stacked flat cylinders, with the position of the global and local axis.

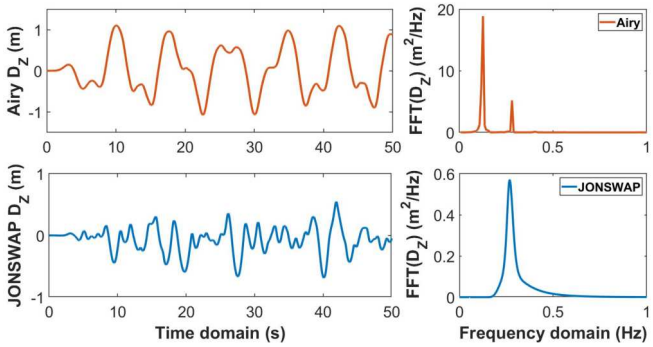


Fig. 9. Simulated drifter vertical displac ement ($D_Z$) using two different sea models; orange has been used for Airy model and blue for JONSWAP model. The left side of the figure contains the time domain and the right side contains the frequency domain.

frequency as its FFT results present two peaks, one at around 0.3 Hz ($1/T_{Z1}$) and the second at around 0.12 Hz ($1/T_{Z2}$). Its time-domain peak-to-peak amplitude can reach up to 2 m when both waves align. JONSWAP $D_Z$ presents a lower amplitude than Airy's because its main $H_{S3}$ is smaller than the composition of $H_{S1}$ and $H_{S2}$. Its frequency-domain results present a frequency distribution around $1/T_{Z3}$ instead of a peak centered in a single frequency.

### *B. FEA simulation results*

Under the base excitation with drifter motions patterns shown in Fig. 9, the displacement response of the device in the time domain are obtained and presented in Fig. 10. Since the displacement amplitude of the drifter motion patterns are in meters and it is much larger than the dimensions of the SBCM, the displacement curves of the base and mass are almost overlapped with each other as shown in Fig. 10 (a) and Fig. 10 (c). Therefore, relative displacement curves between the frame and the mass block are presented separately for a clear illustration in Fig. 10 (b) and Fig. 10 (d). It is shown that the maximum relative displacement amplitude between the base and mass of the SBCM in the Airy ocean wave is about 9 mm. In the Jonswap ocean wave, the maximum relative displacement amplitude reaches about 10 mm. According to the FEA simulation results, the SBCM designed shows good sensitivity to the ocean waves when it is embedded into drifters to be used as a WEC.

Excited by the drifter motion patterns, voltage outputs across the external resistance are generated in the FEA simulation. The Voltage curves and the calculated instantaneous power curves with respect to time are plotted in Fig. 10 (e) – (h). The relative displacement between the mass and the frame is also plotted in the individual figures as references to highlight the relationship between the deformation of the beams and the piezoelectric output voltage. Fig. 10 (e) shows that the AC voltage reaches the maximum of 1.37 V in the excitation condition corresponding to the synthesized airy ocean wave. The maximum instantaneous power is about 1.87 μW as shown in Fig. 10 (f). In the excitation condition corresponding to the Jonswap ocean wave, the maximum AC voltage is about 1.53 V (as shown in Fig. 10 (g)) and the maximum instantaneous power is about 2.34 μW (as shown in Fig. 10 (h)). The electric generation capability of the preliminary SBCM-based PVEH under ocean wave excitations is verified with the FEA simulations in the time domain though the voltage outputs. Instantaneous power dissipated over the load is low due to the non-optimized electric loads and the piezoelectric attachment positions.

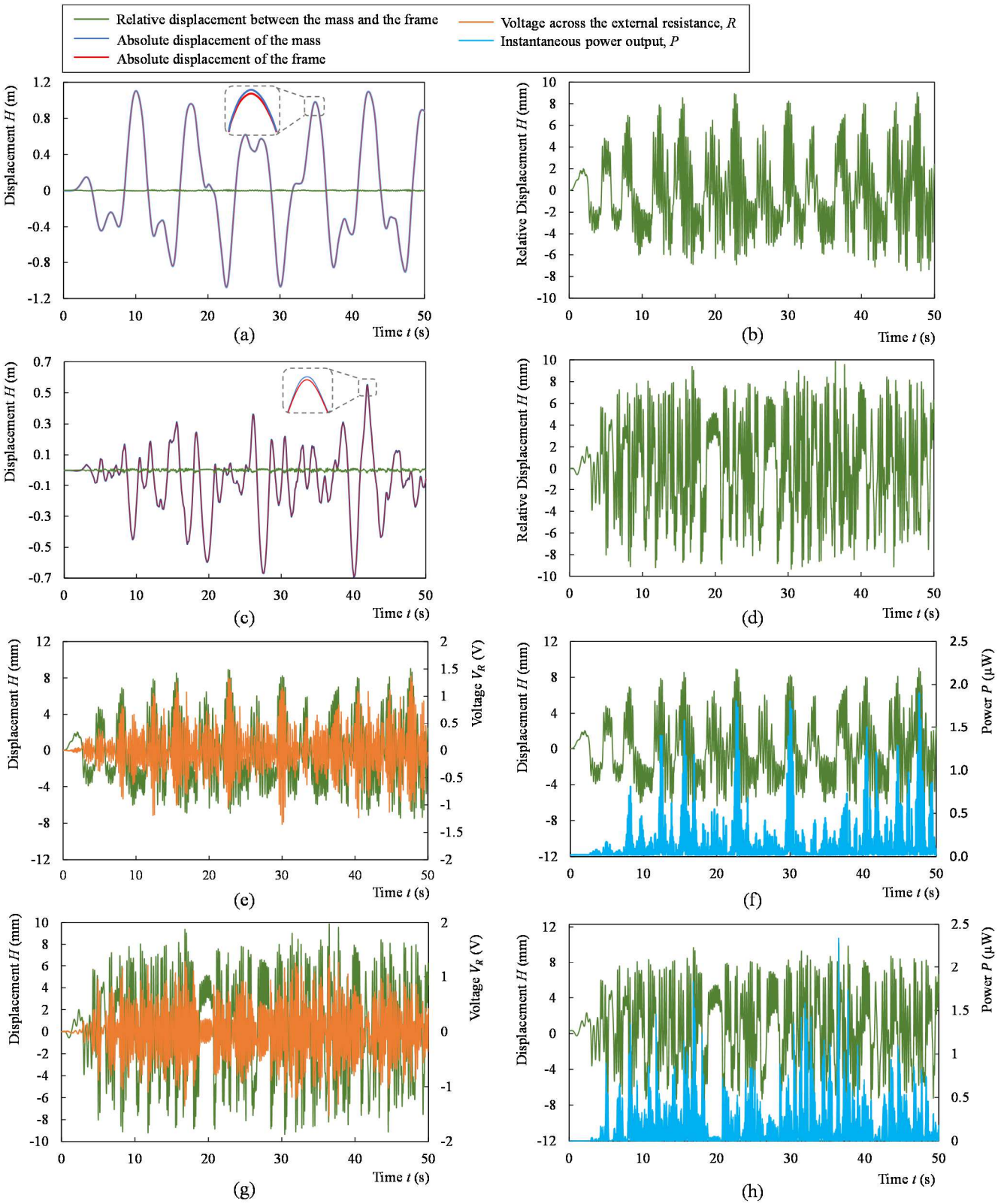


Fig. 10. FEA simulation results of the displacement response of the SBCM. (a) Absolute displacements of the frame and mass block and (b) The relative displacement between the frame and the mass block excited by the drifter motion pattern corresponding to ocean wave A; (c) Absolute displacements of the frame and mass block and (d) The relative displacement between the frame and the mass block excited by the drifter motion pattern corresponding to ocean wave B. Right side; (e) Voltage output across the load resistance and (f) Instantaneous power generated over the external resistance together with the relative displacement between the base and mass under the base excitation corresponding to the synthesized airy ocean wave in time domain; (g) Voltage output across the load resistance and (h) Instantaneous power generated over the external resistance together with the relative displacement between the base and mass under the base excitation corresponding to the Jonswap ocean wave in time domain.

## V. Conclusions

Ocean waves have mixed frequencies in the low frequency range with weak accelerations. The SBCM provides a structural solution for WECs. The dynamic response of the SBCM to harmonic base excitations with ultra-low excitation frequencies is investigated based on time-domain FEA simulations. The applicability of the SBCM in harvesting energy from ocean waves is then demonstrated with PVDF films added in the FEA model. Using the drifter motion patterns driven by two typical ocean waves, the displacement response and electric outputs are observed in the FEA simulations. Conclusions are drawn as follows.

1) The SBCM responds to an ultra-low excitation frequencies in a wide frequency range, which has been verified by the FEA simulations, analytical results and numerical analysis with a close agreement.

2) According to the electric output generated at the preliminary SBCM-based PVEH, the SBCM can embedded into a drifter as a WEC to harvest energy from ocean waves.

Future work includes FEA simulation of the SBCM under drifter rotational excitations (pitch and roll), experimental integration of the SBCM prototype with the ocean drifter and real sea test, optimization on the electric circuits etc.

## Acknowledgment

This research is financially supported by the project of EnABLES. EnABLES (http://www.enables-project.eu/) has received funding from the EU Horizon 2020 research & innovation programme, under Grant Agreement No. 730957. The authors extend their gratitude to Orcina for their kind support and offer of the academic license OrcaFlex N2703 (2021) to Universitat Politècnica de Catalunya.

## References

[1] J. Del-Rio *et al.*, "Obsea : A Decadal Balance for a Cabled Observatory Deployment," *IEEE Access*, pp. 33163–33177, 2020.

[2] S. Gomáriz, I. Masmitjà, J. González, G. Masmitjà, and J. Prat, "GUANAY-II: an autonomous underwater vehicle for vertical/horizontal sampling," *J. Mar. Sci. Technol.*, vol. 20, no. 1, pp. 81–93, 2015.

[3] "MELOA project." [Online]. Available: https://www.ec-meloa.eu/. [Accessed: 21-Oct-2021].

[4] R. Lumpkin, T. Özgökmen, and L. Centurioni, "Advances in the Application of Surface Drifters," *Ann. Rev. Mar. Sci.*, vol. 9, no. 1, pp. 59–81, 2017.

[5] P. M. Poulain, R. Gerin, E. Mauri, and R. Pennel, "Wind effects on drogued and undrogued drifters in the eastern Mediterranean," *J. Atmos. Ocean. Technol.*, vol. 26, no. 6, pp. 1144–1156, 2009.

[6] W. Ding, B. Song, Z. Mao, and K. Wang, "Experimental investigation on an ocean kinetic energy harvester for underwater gliders," in *IEEE Energ. Conv. Congr. and Expos. - Montreal*, 2015, pp. 1035–1038.

[7] G. Bracco, A. Cagninei, E. Giorcelli, G. Mattiazzo, D. Poggi, and M. Raffero, "Experimental validation of the ISWEC wave to PTO model," *Ocean Eng.*, vol. 120, pp. 40–51, 2016.

[8] Y. Li *et al.*, "Study of an Electromagnetic Ocean Wave Energy Harvester Driven by an Efficient Swing Body Toward the Self-Powered Ocean Buoy Application," *IEEE Access*, vol. 7, pp. 129758–129769, 2019.

[9] W. Ding, K. Wang, Z. Mao, and H. Cao, "Layout optimization of an inertial energy harvester for miniature underwater mooring platforms," *Mar. Struct.*, vol. 69, no. 102681, p. 17, 2020.

[10] M. Carandell, D. M. Toma, M. Carbonell, J. del Río, and M. Gasulla, "Design and Testing of a Kinetic Energy Harvester Embedded into an Oceanic Drifter," *IEEE Sens. J.*, 2020.

[11] M. Carandell, D. M. Toma, J. P. Pinto, M. Gasulla, and J. del Río, "Impact on the Wave Parameters Estimation of a Kinetic Energy Harvester Embedded into a Drifter," in *OCEANS - Singapur and U.S. Gulf Coast*, 2020.

[12] N. V Viet, N. Wu, and Q. Wang, "A review on energy harvesting from ocean waves by piezoelectric technology," *J. Model. Mech. Mater.*, vol. 1, no. 2, 2017.

[13] H. Liang, G. Hao, and O. Z. Olszewski, "A review on vibration-based piezoelectric energy harvesting from the aspect of compliant mechanisms," *Sensors Actuators, A Phys.*, vol. 331, p. 112743, 2021.

[14] L. L. Howell, *Compilant Mechanisms*. JOHN WILEY & SONS, INC, 2001.

[15] G. Hao, X. Kong, and R. L. Reuben, "A nonlinear analysis of spatial compliant parallel modules: Multi-beam modules," *Mech. Mach. Theory*, vol. 46, no. 5, pp. 680–706, 2011.

[16] G. Hao, "A framework of designing compliant mechanisms with nonlinear stiffness characteristics," *Microsyst. Technol.*, vol. 24, no. 4, pp. 1795–1802, 2018.

[17] G. Hao, J. Yu, and H. Li, "A brief review on nonlinear modeling methods and applications of compliant mechanisms," *Front. Mech. Eng.*, vol. 11, no. 2, pp. 119–128, 2016.

[18] W. H. Munk, *Origin and generation of waves*. Scripps Institution of Oceanography La Jolla Calif, 1951.

[19] Z. Demerbilek, "Water Wave Mechanics," in *Coastal Engineering Manual*, vol. Part II, 2008.

[20] R. M. Isherwood, "A revised parameterisation of the Jonswap spectrum," *Appl. Ocean Res.*, vol. 9.1, pp. 47–50, 1987.